MACHINE ELEMENT CONTRIBUTION TO THE LONGITUDINAL IMPEDANCE MODEL OF THE CERN SPS

T. Kaltenbacher*, F. Caspers, C. Vollinger
CERN, Geneva, Switzerland

Abstract

This contribution describes the current longitudinal impedance model of the SPS and studies carried out in order to improve, extend and update it. Specifically, new sources of impedances have been identified, evaluated and included in the model. One finding are low Q and low-frequency (LF; here below 1 GHz) resonances which occur due to enamelled flanges in combination with external cabling e.g. ground loops. These resonances couple to the beam through the gap with enamel coating which creates an open resonator. Since this impedance is important for beam stability in the CERN Proton Synchrotron (PS), RF by-passes were installed on the enamelled flanges, and their significance for the SPS beam is currently under investigation. Simulations, bench and beam measurements were used to deduce model parameters for beam dynamic simulations.

INTRODUCTION

A significant SPS upgrade is mandatory in order to meet the expectations for the planned LHC upgrade scenarios [1] since there are still intensity limitations apparent for future high-intensity LHC beams [2, 3]. Beam measurements and the current longitudinal beam coupling impedance model of the SPS [4] have unveiled the main contributors to the resistive impedance which are vacuum flanges, and the 200 MHz cavities to name but a few. The main contributor to the high R/Q impedances are the kicker magnets and again the 200 MHz cavities [3].

Vacuum flanges in the SPS were found to be responsible for single- and multi-bunch longitudinal instabilities. Therefore, an impedance reduction campaign of these vacuum flanges (VF) during the Long Shutdown 2 (LS2 in 2019) is LIU baseline. However, it is not yet clear if the flange insulation has to be maintained or not. In order to answer this question, a campaign is planned during a technical stop in 2016 [5] to shortcircuit all insulated VF of the 109 QF (quadrupole focusing magnet) short straight sections (SSS) by so-called soft clamps. Detailed beam parameter measurements before and after the deployment of these soft clamps will provide the basis for the decision whether the VF can maintain their enamel insulation or not. Based on this decision, the current flange shield design for impedance reduction will have to be reviewed or can be kept. This is very important, since many of the positions that have to be shielded are equipped with enamelled flanges. In the PS [6], insulated vacuum flanges are used to avoid eddy currents induced by fast ramping (ramp rates $\approx$ 2.3 T/s) of C-shaped magnet , and to avoid that ground loops are closed via the beam pipe. From measurements, it could be shown that the flange capacitance and the connected CBN (ground loops) form a resonator with a resonant frequency of about 1.5 MHz which had to be dampened with by means of RF-bypasses. As before for the PS, also in the SPS, the enamelled flanges were introduced to avoid eddy current propagation along the beam pipe, and in addition to allow a sectorising of the vacuum system such that only *one* ground connection is installed at each half-cell (approx. every 32 m). In the SPS however, the ramping rates of H-window magnets are about 10 times slower than in the PS and induced net currents on the beam pipe are thus considerably smaller as well. From laboratory measurements, it could be shown that the induced current from focusing quadrupole magnets (QF) is below 1.5 A and from defocusing quadrupole magnets (QD) less than 200 mA. In addition, from measurements, it could be shown that in the SPS, a resonator which is formed by the flange capacitance and the ground loop, is resonating at about 2.5 MHz. The same measurements also indicated a number of resonances at higher frequencies, i.e. at about 20 MHz, about 60 MHz, and higher. It should be mentioned already here that these resonances show a spread around the indicated frequencies due to slight variations in the grounding loop lengths and topology, as is illustrated in Fig. 1. Consequently, the current impedance model has to be extended to include these low-frequency resonances occurring due to enamelled flanges.

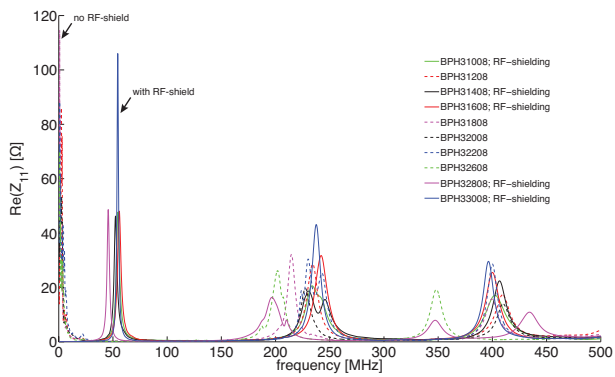

Figure 1: Differentially measured reflection coefficient S_{11} was used to calculated the real part of input impedance Z_i - $Re(Z_i)$ - of 10 QF SSS with and without RF-shield.

MEASUREMENTS

In order to evaluate these low frequency resonances, two different type of measurements were performed with a vector network analyser (VNA) in the SPS. Firstly, measurements of reflection S-parameters (S_{11}) were carried out to obtain

* Thomas.Kaltenbacher@cern.ch

ISBN 978-3-95450-178-6

the low-frequency input impedance of enamelled flanges, and secondly we performed measurements via a pick-up (PU) installation. The PU consisted of conducting loops that are connected to an inner and outer conductor of a coaxial cable and were put in place to the left and right side of the flanges. Via the PU installation, beam induced measurements from the surface were possible. Again, reflection S-parameters were taken as read-out signal to allow an evaluation in the same manner as for the first set of data. In order to rule out spurious signals caused by coupling effects due to the surrounding installation, independent *differential* RF measurements were performed for the very same positions. These single-ended and differential measurements, as well as the beam induced measurement set-ups are described in more detail below together with their results.

RF Measurements

For the single-ended (s.e.) RF measurement, the VNA was connected to the pick-up (PU) by means of a BNC-N adapter (see Fig. 2). During the measurements, we could determine that the upper signal frequency limit of the s.e. RF measurement to a value of about 30 MHz, caused by the coupling of the outer conductor of the cable to other electrical installations and equipment, i.e. the EM surrounding.

The differential (diff.) RF measurement method was applied using a hybrid junction (MACOM H-9-N; nominal bandwidth 2 to 2000 MHz) [7]. Two RF measurement cables with pins connected to them (see Fig. 3) and provided an independent measurement of the very same pick-up.

Figure 2: Pick-up (PU3) position in the short straight section of the focusing quadrupole magnet QF31610 in the SPS.

Via the hybrid, signals between the 0° and 180° phase shift port were taken. It is worthwhile to mention that both cables were calibrated simultaneously by means of a one-port calibration and that the differential characteristic impedance is 100 Ω. This characteristic impedance was used to convert the reflection coefficient S_{11} to the input impedance (Z_i). As expected, this set-up is limited towards low frequencies at about 1 MHz, when spurious signals caused by data interpolation as well as calibration effects of the VNA become visible. Also, operation of the hybrid junction below 2 MHz is difficult, so that we did not consider these very low frequency values. The upper frequency limit shows up at about 500 MHz and is caused by increased loss from contact resistance and signal interferences.

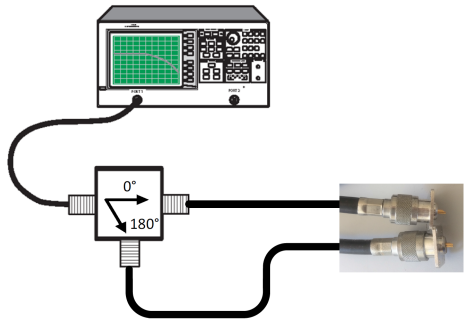

Figure 3: Schematic of differential RF measurement set-up.

Beam Induced Measurements

In order to show the coupling of the beam to the EM surrounding through enamelled flanges, beam induced measurements were performed. Three positions with enamelled flanges were chosen (PU1 to PU3) and fitted with to so-called soft clamps. These clamps are tailor-made from copper braids into which cable ties were slid similar to a sleeve. The cable ties allowed to strap the soft-clamp on the beam pipe to the left and right side of the flange. A socket was soldered on each of the clamps beforehand and the PU was completed by connecting the clamps with a banana-BNC adapter (see Fig. 2) which in turn was connected to a spare coaxial cable running from the tunnel to the surface. Such a pick-up represents a single-ended measurement of the (beam) induced signal across a VF. The signals were acquired one second after injection with a fast, high analogue band-width oscilloscope with 50 ps time sampling period and afterwards converted to frequency domain by means of fast Fourier transform (FFT). Although in the SPS, the single bunch beam (with bunch length $4\sigma_t \approx 3$ ns) had a nominal intensity of 1×10^{11} protons per bunch (ppb), all measured data traces except one were taken with 4×10^{10} pbb due to the availability of the cycle during our measurements. Figure 4 shows the spectra of beam induced signals for the three pick-ups (PU1 to PU3) in different locations. Note that for PU3, two traces taken with different intensities are shown and the magnitude scales accordingly ($\approx 10/4$).

SIMULATIONS

Macro-Particle Longitudinal Beam Dynamics

Longitudinal beam dynamics simulations with BLonD [8] were performed with the updated impedance model for the SPS including the scattered LF contribution (see Fig. 1). Two kind of simulations were performed. Firstly, a 72 bunch beam with 25 ns spacing during the ramp, and secondly a synchrotron frequency shift simulation from quadrupole

ISBN 978-3-95450-178-6

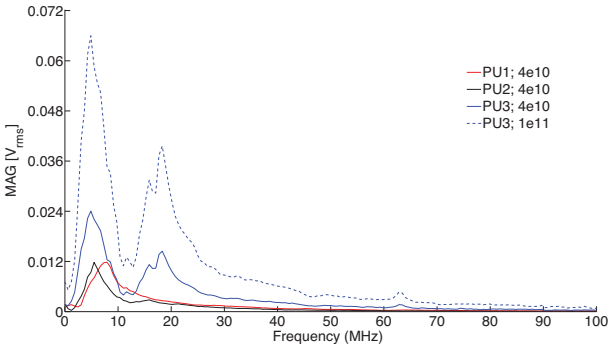

Figure 4: Single-ended spectrum of the beam induced measurements for pick-up PU1 to PU3. Note that the magnitude scales as expected for PU3 by about 2.75 (theoretically 10/4=2.5).

oscillations. Preliminary results have shown that there seems to be no significant effect on neither beam stability nor on the synchrotron frequency shift due to short bunch length [9].

EM Simulation

Figure 5 shows a simplified model of an MBA/MBA flange interface with 4-convolution bellows (undulation was not modelled). This model was used to show the coupling of a TEM signal excited on a wire (1 mm diameter) along the beam axis in order to mimic a wire measurement.

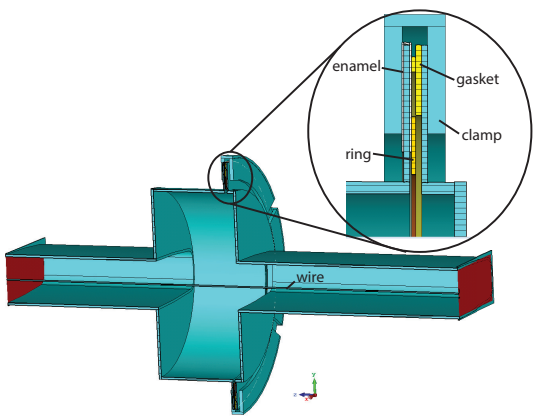

Figure 5: CST model of the simplified MBA/MBA flange structure with bellows and clamp. Note the wire along the beam axis is touching both microwave ports (red).

This special simulation approach was used since wake field simulations did not show any coupling to LF resonances. From our simulations, we see that the aspect ratio of enamel thickness (i.e. opening for coupling) and the VF object dimensions are so extreme that the VF opening remains undetected in the time domain solver. However, the HF solver of CST Microwave Studio [10], was used for S-parameter simulations (HF solver) of the simplified insulated flange structure. It is important to note that the object was embedded in vacuum so that the metal structure of the flange and beam pipe did no touch the perfect electric conducting (PEC) boundaries. This way modes from the inside are allowed to couple to the outside of the structure through the enamel layer (300 µm thick) via the clamp (see Fig. 6). In the Results and Conclusion section will be shown how the coupling takes place in the simulation.

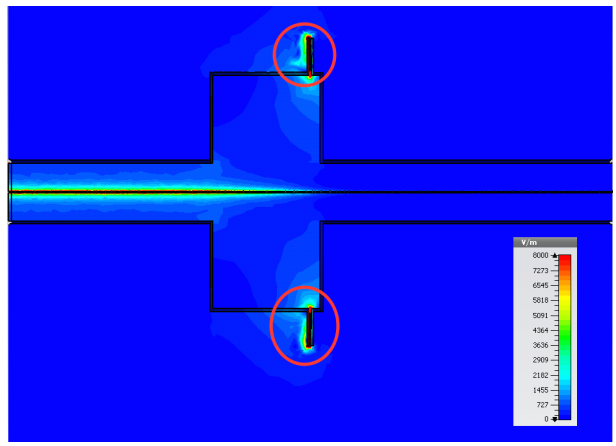

Figure 6: E-field magnitude of the mode at 13.8 MHz of the model shown in Fig. 5 with $\mu_r = 50$. Note the coupling to the surrounding through the VF including the gasket and enamel (red circles).

RESULTS

Beam Induced Measurement Results

The method of beam induced measurements was evaluated for the three pick-ups shown in Fig. 4. All three positions show a significant peak below 10 MHz which is most likely caused by resonance of the VF capacitance and the common bounding network (CBN). Furthermore, the spectrum of PU3 shows also significant peaks around 18 and 62 MHz which coincide with resonances measured differentially at the very same position.

RF Measurement Results

As explained in the introduction, RF-shields were installed in about 860 intermagnet pumping ports during the impedance reduction campaign in the year 2000 [11], however, detailed documentation is sometimes missing or unreliable for some positions. Thus, as a first exercise measurements of the input impedance from S-parameter on QF SSS at the beam monitor position were carried out in order to deduce whether an RF-shield is installed at a certain position or not. As expected, in locations known to be equipped with RF-shields, the first resonance appears at approx. 60 MHz whereas at locations known to be without RF-shields, the first resonance is measured at about 10 MHz (see Fig. 1).

As a next step, this method was used in the locations of the pick-ups in order to allow a comparison of input impedances measured by the s.e. and diff. methods as is shown in Fig. 7 for pick-up nr. 3. Note that pick-up nr. 3 is installed in the SSS of magnet QF31610 (see Fig. 2). For the s.e. measurement the two variations of the connections, the outer conductor

ISBN 978-3-95450-178-6

(GND) of the coaxial cable to the right or left of the VF, are shown. The data shows an increasing input impedance below 5 MHz which could be attributed to the independently evaluated flange capacitance of about 600 pF. From the measurement of input impedance with the s.e. method, we observe an increase above 20 MHz due to the capacitive coupling of the coaxial cable to the (EM) surrounding. Qualitatively both measurement methods agree very well with each other and the beam induced signal shows an excellent agreement with the differentially measured impedance.

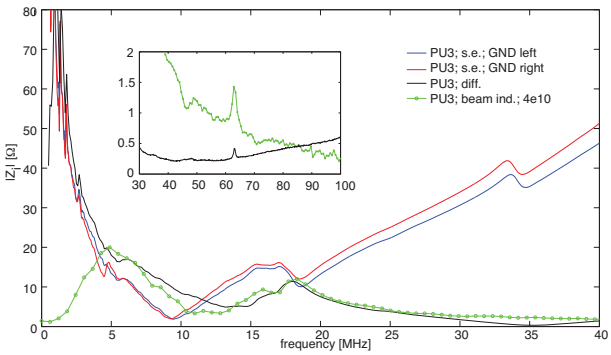

Figure 7: Measurement results for pick-up (PU3) including the impedance by single-ended (s.e.) and differential (diff.) method. GND left and right describes the configuration where the outer conductor of the coax. cable was connected to with respect to the VF. The beam induced (beam ind.) spectrum for a single bunch beam with an intensity of 4×10^{10} protons is scaled to match the impedance values. Inset: Zoom on resonance at 62 MHz from beam induced measurement (green) and diff. RF measurement (black).

EM Simulation Results

Figure 8 shows the transmission signal S_{21} from the simulated flange model presented in Fig. 5. From the simulations, we observe a significant dip at about 1.64 GHz which could be attributed to a strong coupling of the flange to the outside through the enamel layer, even if the fixation clamp is absent in the model. Adding the clamp in the model causes the dip to scatter due to a build-up of EM-fields that are leaking to the outside at the clamp position. A large variation of the EM surrounding exists in the SPS and causes a varying inductance of ground loops at the enamelled VF positions. In order to include this EM surroundings in our simulation model, an additional ring was inserted at the gasket location to mimic the EM environment, and different material properties were assigned to this ring. The simulation results show that the variation of material properties of the ring (relative permeability μ_r and permittivity ε_r) cause a shift of the resonance frequencies towards lower values, and thus provide a simulation model for the EM situation in the SPS at the VF positions. The successful description of measurement data by simulations is the base for further studies concerning the beam coupling to the shown LF resonances.

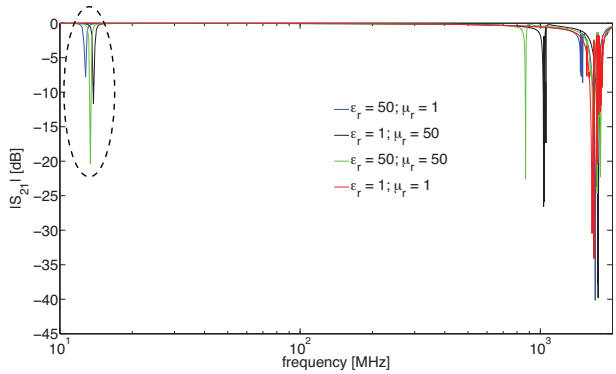

Figure 8: Simulated transmission S-parameter (S_{21}) for the simplified flange model shown in Fig. 5 with μ_r and ε_r variation assigned to a ring that was inserted next to the gasket (see Fig. 5). The shifted LF resonances are highlighted.

CONCLUSION

In this work we have introduced and evaluated LF resonances connected to enamelled vacuum flanges in the SPS. This allowed us to update the current SPS impedance model and to analyse the additional contribution in terms of beam coupling impedances. Furthermore, a simplified simulation model of the VF was proposed in order to describe and reproduce coupling from the flange inside to the outside EM surrounding. Beam dynamic simulations could not point out any significant effect neither on the stability threshold of a multi-bunch beam not on the synchrotron frequency shift. However, further studies will be carried out to qualify the significance of this coupling by performing further EM and beam dynamics simulations.

ACKNOWLEDGEMENT

We are grateful to our RF colleagues T. Bohl for his support during the beam induced measurements and the pick-up installation in the SPS, E. Shaposhnikova, and J. F. Esteban-Müller for their useful inputs and discussions. We would like to thank also A. Lasheen and J. Repond for their beam dynamics simulation and P. Kramer for his support during the measurements in the SPS.

REFERENCES

[1] J. Coupard *et al.*, "LHC Injectors Upgrade, Technical Design Report, Vol. I: Protons", Dec. 2014

[2] T. Argyropoulos *et al.*, "Identification of the SPS impedance at 1.4 GHz", in *Proc. 4th Int. Particle Accelerator Conf. (IPAC'13)*, Shanghai, China, May 2015, paper TUPWA039, pp. 1793–1795.

[3] E. Shaposhnikova *et al.*, "Identification of high-frequency resonant impedance in the CERN SPS", in *Proc. 5th Int. Particle Accelerator Conf. (IPAC'14)*, Dresden, Germany, June 2014, paper TUPME029, pp. 1416–1418.

[4] J. E. Varela *et al.*, "An extended SPS longitudinal impedance model", in *Proc. 6th Int. Particle Accelerator Conf. (IPAC'15)*, Richmond, USA, May 2015, paper MOPJE035, pp. 360–362.

ISBN 978-3-95450-178-6

[5] B. Goddard, presentation at 173rd IEFC meeting on 20th May 2014, https://indico.cern.ch/.

[6] H. Damerau *et al.*, "Evaluation of the broadband longitudinal impedance of the CERN PS", CERN, Geneva, Switzerland, CERN-ATS-Note-2012-064 MD, May 2012.

[7] MACOM Technology Solutions Inc., Lowell, USA, http://cdn.macom.com/datasheets/H-9.pdf.

[8] BLonD, Beam Longitudinal Dynamics code, http://blond.web.cern.ch.

[9] A. Lasheen and J. Repond, private communication

[10] CST AG, Darmstadt, Germany, http://www.cst.com

[11] P. Collier and A. Spinks, "Survey of the Short Straight Sections in the SPS for the Impedance Reduction Programme", CERN, Geneva, Switzerland, SL-Note-99-025 SLI, April 1999.

ISBN 978-3-95450-178-6